Effect of Curing Time on The Pore Size and Effective Thickness/Porosity of Polyester Thin Film Composite Nanofiltration Membranes

K. H. Mah[a], H. W. Yussof[a*], M. N. Abu Seman[a], A. W. Mohammad[b]

[a]Faculty of Chemical & Natural Resources Engineering, Universiti Malaysia Pahang, 26300, Kuantan, Pahang, Malaysia
[b]Department of Chemical and Process Engineering, Faculty of Engineering and Built Environment, Universiti Kebangsaan Malaysia, 43600, Bangi, Selangor, Malaysia

Graphical abstract
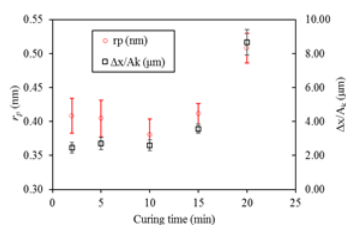
Abstract

Polyester thin film composite nanofiltration membranes were synthesized on the polyethersulfone (PES) support via the interfacial polymerization between triethanolamine (TEOA) and trimesoyl chloride (TMC). Here we report the effect of curing time in the interfacial polymerization process on membrane properties like pore size and effective thickness/porosity. The membrane properties were determined based on the uncharged solute permeation test and the hypothetical mechanistic structure (pore size, effective thickness/porosity) was determined using Donnan steric pore flow model (DSPM). This study also provides information on the effect of curing time on water permeability. From the 2 minute point to 10 minute point, the membranes pore sizes were reduced and negligible changes to effective thickness/porosity suggest the occurrence of additional cross-linking reaction between aqueous and organic monomers.

Keywords: Thin-film composite membrane, interfacial polymerization, curing time, pore size, effective thickness/porosity

Abstrak

Membran komposit film nipis nanoturasan telah disintesis keatas sokongan polietersulfon melalui pempolimeran antara muka menggunakan trietanolamina dan trimesoyl klorida. Disini kami melaporkan kesan masa pengawetan dalam proses pempolimeran antara muka keatas sifat-sifat membran seperti saiz liang dan ketebalan/keliangan berkesan. Sifat-sifat membrane ditentukan berdasarkan ujian turasan zat terlarut tidak bercas dan struktur mekanikal hipotesis (saiz liang, ketebalan/keliangan berkesan) ditentukan menggunakan model aliran liang Donnan sterik. Kajian ini juga memberi informasi mengenai kesan masa pengawetan ke atas ketelapan air. Dari titik 2 minit ke titik 10 minit, saiz liang membrane mengecut dan perubahan boleh abai ke atas ketebalan/keliangan berkesan mencadangkan berlakunya tindakbalas silang cantum diantara monomer akueus dan organik.

Kata kunci: Membran komposit filem nipis, pempolimeran antara muka, masa pengawetan, saiz liang, ketebalan/keliangan berkesan

1.0 INTRODUCTION

Xylose is mainly found in the hemi-cellulosic fraction of hardwoods and herbaceous materials. Consequently, hydrolysis is employed to break the long chain of hemicellulose into xylose [1]. Nonetheless, hydrolysis of hemi-cellulosic biomass also produces glucose, another monosaccharide with considerable fraction in hydrolysates, in addition to the xylose [2, 3]. Hence, separation of these monosaccharides is needed to obtain the pure fraction of a specific monosaccharide.

Most of the monosaccharide purification in sugar industry is performed by chromatography due to fairly similar physicochemical properties between monosaccharides. However, chromatography process requires a large amount of time, resources (usually water use for eluent), and energy [4]. Alternatively, commercial NF membrane has demonstrated the ability to separate xylose and glucose from a xylose-glucose mixture [5], which later applied in different hemicellulose hydrolysate [6]. These finding brought the separation of xylose from glucose toward a new direction, with the possible use of membrane in separating xylose from glucose. Separation of xylose from glucose in these past studies have very good performance with xylose separation factor between 1.5 – 3.0.

In our previous study, we attempted to produce self-made TFC membrane via interfacial polymerization for separating xylose from glucose, using TEOA and TMC as monomer on polyethersulfone (PES) ultrafitration membrane. The self-made TFC membrane proved to be able to separate xylose from glucose with the highest xylose separation factor achieved at 1.64 comparable with commercial membrane. [7]. From our previous study, curing was found to have a large influence on the membrane performance. Curing in IP relies on the temperature and duration of the film are exposed to. Curing TFC membrane near the organic solvent's boiling point is highly favourable due to the high flux and rejection [8, 9], However, many studies reported the best curing time using hexane as an organic solvent varies from 55 seconds [9], 3 minutes [10], 10 minutes [8,11], to 15 minutes [12]. It should be also noted, most of these study employed different monomers in their interfacial polymerization.

Study on the effect of curing time in interfacial polymerization on membrane performances, namely pure water flux, permeation flux, and xylose separation factor have been performed and reported elsewhere [13]. This paper aims to add information on the effect of curing time in the interfacial polymerization process on membrane properties like pore size and effective thickness/porosity. This study also provides information on the effect of curing time toward water permeability.

2.0 METHODOLOGY

2.1 Material

The asymmetric commercial PES membrane was purchased from AMFOR Inc. (China) with the commercial name of UF PES50. The membrane has a nominal molecular cut-off of 50 kDa and water flux (at 25 °C) of 260 LMH. The chemicals used in this study were triethanolamine (R & M Marketing, Essex, UK), trimesoyl chloride (Alfa Aesar, UK), sodium hydroxide (Merck, Germany), n-hexane (Merck, Germany), xylose (Sigma Aldrich, USA), glucose (Sigma Aldrich, USA), and acetonenitrile (J.T. Baker, USA). All chemicals were analytical grade with high purity (> 99%) and acetonitrile with High Performance Liquid Chromatography (HPLC) grade.

2.2 Preparation of TFC Membrane

The polyester TFC membrane was developed using interfacial polymerization technique based on previous studies [14, 15] with slight modification . 1×10^{-6} M sodium hydroxide aqueous solution was prepared as the base medium for aqueous phase monomer solution. The aqueous phase monomer solution was then prepared by dissolving 4 % (w/v) of TEOA with the base medium. The organic monomer phase solution was prepared by dissolving 0.25 % (w/v) of TMC in pure hexane. The commercial PES support membranes were cut into disc shape and pre-treated before initiating the interfacial polymerization process. The PES membranes were firstly soaked in ultrapure water for at least 12 hours, then treated with ultrasonification for 6 minutes in ultrasonic bath to remove glycerine preserving the pores. Interfacial polymerization process was started by soaking the commercial PES support membrane in the aqueous phase monomer solution for a period of 30 minutes. After that, the membrane was then drained and rolled with a glass rod to remove excess liquid on top of a flat glass surface. Then, the membrane was immersed in the organic phase solution for a period of 45 minutes. Finally, the TFC membranes were dried in an oven (UF 55, Memmert, USA) at 60 °C for 2, 5, 10, 15, and 20 minutes.

2.3 Nanofiltration Set-Up and Permeation Experiments

Nanofiltration experiments have been carried out using the stirred cell system schematized in Figure 1. A Millipore stirred cell (Model 8200, Millipore-Amicon Corporation, USA) having a maximum volume uptake of 200 mL and an effective membrane area of 2.87×10^{-3} m^2 was used in all experiments. Prepared TFC membrane and virgin PES membrane was fitted into the membrane holder at the bottom of the stirred cell. Other parts are then assembled together and place on top of a magnetic stirrer

(Model MS-20D, Daihan Scientific Co. Ltd., South Korea).

Nitrogen gas
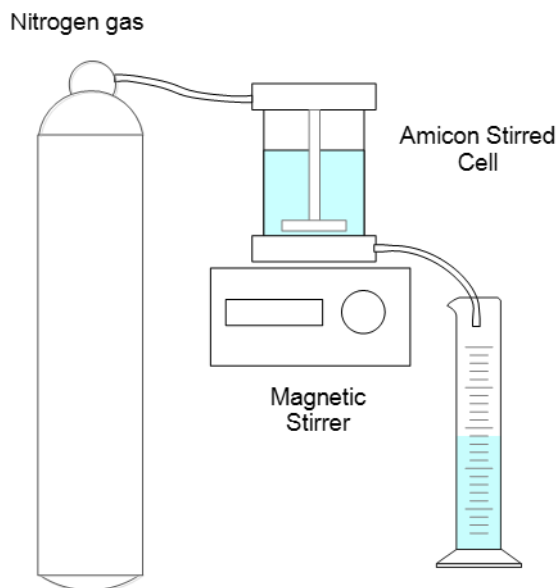
Figure 1 Schematic diagram of nanofiltration system

180 mL of ultrapure water was poured into the stirred cell. Pure water flux experiment was performed at different pressure (2, 3, and 4 bar) by measuring the time taken for 20 mL of ultrapure water collected with constant stirring speed of 300 rpm using nanofiltration set-up mentioned. After that, a xylose-glucose mixture solution for sugar filtration was prepared by dissolving 5 g of xylose and 5 g of glucose in 1 L of deionized water. This mixture gives concentration of 5 g/L of xylose and 5 g/L of glucose. 180 mL of the xylose-glucose mixture solution was filled into the stirred cell. The nanofiltration was performed by collecting 20 mL of permeate at pressure 4 bar and stirring speed of 300 rpm at room temperature. The duration for the permeate to reach 20 mL were measured to calculate xylose-glucose mixture flux, J_v. After the nanofiltration, the composite membrane was flushed by deionized water at a stirring speed of 350 rpm for 30 minutes, without applying any pressure. Fluxes in this work was calculated using the following equation:

$$J_i = \frac{\Delta V}{A.\Delta t} \tag{1}$$

where J_i denoted as J_w and J_v for pure water and xylose-glucose mixture solution fluxes, respectively, ΔV is the total volume of the permeate collected (0.02 L), Δt is the duration taken to collect 20 mL of permeate in hour, and A is the effective area of the membrane (2.87 x 10^{-3} m^2). A pure water fluxes against applied pressure graph was plotted to find the pure water permeability, P_m. The gradient for fitted linear lines with 0 as intercept was the P_m for the

respective membranes. The observed solute rejection, R_{obs} rates of the TFC membranes were calculated using the following equations:

$$R_{obs} = 1 - \frac{C_p}{C_b} \tag{2}$$

$$C_b = \frac{C_f + C_r}{2} \tag{3}$$

where C_p is the concentration of respective solute in permeate (g/100 g of solution), C_b is the concentration of respective solute in bulk (g/100 g of solution), C_f is the concentration of respective solute in feed (g/100 g of solution), and C_r is the concentration of respective solute in retentate (g/100 g of solution).

2.4 Quantification of Sugar using High Performance Liquid Chromatography (HPLC)

Quantification of samples was done using HPLC (1200 Series, Agilent Technologies, USA) equipped with refractive index detector. The liquid chromatography column used in this study was Agilent's Zorbax Carbohydrate 5 µm (4.6 × 250 mm) with an operating flow rate of 1 mL/min and injection volume of 20 µL. The mobile phase used during analysis was prepared by diluting three parts for acetonitrile with one part of ultrapure water. Prior to HPLC analysis, the mobile phase was filtered using nylon membrane with pore size of 0.22 µm and degassed using ultrasonic bath at room temperature for 1 hour. All HPLC samples were filtered using a 3 mL syringe with a 0.2 µm filter attached.

2.5 Determination of Pore Size and Effective Thickness/Porosity

Previous studies have shown the effective pore radius (r_p), and the ratio of effective membrane thickness over porosity for TFC nanofiltration membranes are best characterized using approximate characterization method [16, 17]. The flux and rejection data was fitted using the Donnan-Steric-Pore Model (DSPM) and Hagen- Poiseuille equation.

The DSPM model is based on the extended Nernst–Planck equation expressed below. The model gives the flux of the solute i (j_i) resulting from transport due to diffusion, electrical and convection forces.

$$j_i = -D_{i,p}\frac{dc_i}{dx} - z_i c_i D_{i,p}\frac{F}{RT}\frac{d\psi}{dx} + K_{i,c}c_i v \tag{4}$$

where,

$$D_{i,p} = K_{i,d}D_{i,\infty} \tag{5}$$

For uncharged solute, the transport is governed purely by diffusive and convective flows inside the

membrane thereby reducing the above mentioned Nernst–Planck equation to

$$j_i = -D_{i,p}\frac{dc_i}{dx} + K_{i,c}c_i v \qquad (6)$$

$K_{i,d}$ and $K_{i,c}$ which are functions of the ratio of solute to pore radius (λ), account for the hindrance due to diffusion and convection, respectively. $K_{i,d}$ and $K_{i,c}$ can be related to the hydrodynamic coefficients K^{-1} (enhanced drag) and G (lag coefficient) according to the following equations;

$$K_{i,d} = K^{-1}(\lambda,0) = 1.0 - 2.30\lambda + 1.154\lambda^2 + 0.224\lambda^3 \qquad (7)$$

$$K_{i,c} = G(\lambda,0) = (2-\phi)(1.0 + 0.054\lambda - 0.988\lambda^2 + 0.441\lambda^3) \qquad (8)$$

where,

$$\lambda = \frac{r_p}{r_s} \qquad (9)$$

λ is the ratio of solute radius (r_s) to pore size (r_p) where, λ has the limitation of $0 < \lambda < 0.95$ [18]. $\emptyset$ is the steric terms relating the finite size of the solute and pore size according to the following equation,

$$\phi = (1-\lambda)^2 \qquad (10)$$

In terms of real rejection (R_{real}), Equation (6) becomes

$$R_{real} = 1 - \frac{C_p}{C_m} = 1 - \frac{K_{i,c}\phi}{1-\exp(-Pe_m)[1-\phi K_{i,c}]} \qquad (11)$$

where C_p the concentration of solute in the permeate, and C_m the concentration of solute on the membrane. The Peclet Number (Pe_m) is defined as,

$$Pe_m = \frac{K_{i,c}J_v\Delta x}{K_{i,d}D_{i,\infty}A_k} \qquad (12)$$

where $D_{i,\infty}$ is the bulk diffusivity of solute ($m^2\,s^{-1}$), J_v the volume flux (based on membrane area) ($m\,s^{-1}$), and $\Delta x/A_k$ the ratio of effective membrane thickness over porosity.

$$J_w = \frac{r_p^2\Delta P}{8\mu(\Delta x/A_k)} \qquad (13)$$

where, J_w is the water flux ($m^3\,m^{-2}\,s^{-1}$), ΔP is the applied transmembrane pressure (kPa) and μ is the viscosity of the solution (kPa s).

Concentration polarization equation was employed to find the concentration of solute on the membrane, C_m. For a stirred cell configuration [16], the observed rejection (R_{obs}) was related to the real

rejection by volume flux, J_v and mass transfer coefficient, k in Equation (14) and Equation (15).

$$\ln\left(\frac{1-R_{obs}}{R_{obs}}\right) = \ln\left(\frac{1-R_{real}}{R_{real}}\right) + \frac{J_v}{k} \qquad (14)$$

$$k = 0.23\left(\frac{r_r^2}{v}\right)^{0.567}\left(\frac{v}{D_\infty}\right)^{0.33}\left(\frac{D_\infty}{r_r}\right)\omega^{0.567} \qquad (15)$$

where, r_r are the radius of effective membrane area (m), v the velocity of solute ($m\,s^{-1}$), and ω the stirring speed (rad/s). Table 1 list all the properties needed for calculation. The diffusivity data and Strokes radius were referred from published works [5].

Table 1 Physical properties of monosaccharides and water

Property	Value
r_r	2.68×10^{-2} m
ω	31.41 rad.s^{-1}
v at 25 °C	8.94×10^{-4} m^2.s^{-1}
μ at 25 °C	8.94×10^{-04} Pa.s
$D_{\infty, xylose}$	7.50×10^{-10} m^2.s^{-1}
$D_{\infty, glucose}$	6.73×10^{-10} m^2.s^{-1}
$r_{s, xylose}$ (Strokes radius)	3.25×10^{-10} m
$r_{s, glucose}$ (Strokes radius)	3.65×10^{-10} m
Molecular weight xylose	150.30 g.mol^{-1}
Molecular weight glucose	180.60 g.mol^{-1}

3.0 RESULTS AND DISCUSSION

The effect of curing time on xylose rejection and glucose rejection is shown in Figure 2. It is found that both xylose and glucose rejections were above 90 % from curing time 2 minute to 15 minute. At 20 minute curing time, both xylose and glucose rejection drastically decreased. This may have resulted from the changes to membrane pore size and membrane effective thickness/porosity.
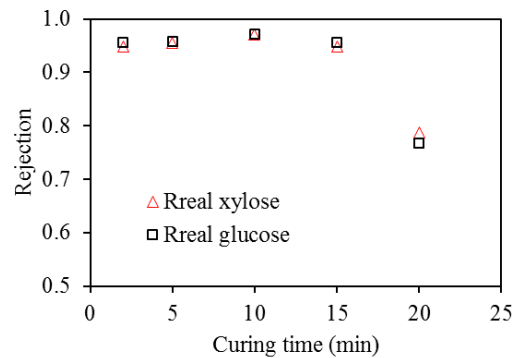
Figure 2 Effect of curing time on xylose and glucose rejection

Figure 3 shows the effect of curing time on membrane pore size and membrane effective thickness/porosity. The membrane pore size and effective thickness/porosity reported in this work were the average of both value calculated from xylose and glucose rejection. Drying of a wet porous material is a very complex process involving thermal equilibrium between solid, moisture and air. Based on the qualitative drying behaviour of microfiltration membrane described by Reingruber *et al.* [19], the first drying level started at the surface of top and bottom side, portrayed by membranes exposed to 2 to 10 minutes of curing in this work. Within this duration, the membrane surface at both top and bottom side were not completely dry due to the transport of both solvents (mostly hexane) from inner part to the surface of membrane through capillary force. This created an interface for additional reaction to occur, hence the decreases in pore size and small increase in thickness/porosity. The additional crosslinking were also promoted through dehydration of unreacted amine and carboxyl groups as explained by Ghosh *et al.* [8].
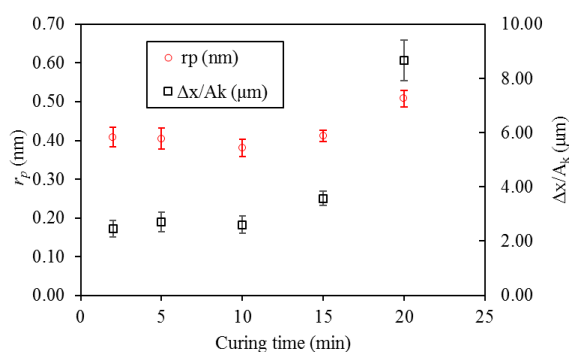
Figure 3 Effect of curing time on membrane pore size, r_p and effective thickness/porosity, $\Delta x/A_k$

From 10 minute until 15 minute of curing time, the drying process enter the next level, where the capillary force within the pores gradually no longer able to transport solvents from inner part to the surface of membrane in some pores. At this level, hexane within the membrane can be presumed to be completely evaporated leaving water behind. Larger pores on the top side (thin-film side) will start to dry up, while smaller pore remain wetted by transport of solvent from inner part using capillary force. At the bottom side (support side), the pores dried up faster than the top side which is in the transition to the next drying level. The pore near the surface of the bottom side started to collapse and transport of solvent from inner part to surface at this side mostly occurred in gaseous state. This occurrence has been describe in the past [19].

The collapse of pores greatly decreases porosity of the membrane as reported in the past [20–22]. Here, it should be noted there was increase in membrane effective thickness/porosity from 10 minute until 15

minute of curing time might be due to the decrease in membrane porosity. The TFC layer formed via interfacial polymerization normally less than 0.2 μm [23]. Although there is increase of pore size and decrease of membrane porosity (increase in effective thickness/porosity) from 10 minute to 15 minute of curing time, the value was not as great as the one from 15 minute to 20 minute of curing time.

The third or last level of drying process were portrayed in membranes cured from 15 minute onwards. The membrane surface was completely dried, while most of the pores in the membrane interior started to dry up sequentially. Then, the solvent within the membrane pores changes to gaseous state (vapour), which later transported to the surface and leave the membrane at both sides of membrane. The porous structure at bottom side of membrane collapsed sharply forming a denser bottom layer, which may have represented by the increase in effective thickness/porosity (decrease in membrane porosity) in Figure 3 from 15 minute to 20 minute point. Increases to membrane pore size from 15 minute point to 20 minute point were not expected. Polyester materials, especially unsaturated polyester are known to shrink up to 1 % when exposed to heat for a certain duration of time [24–26]. The increase of pore size as much as 0.1 nm may have resulted from shrinkage of polyester film layer, stretching the pore outwards making it larger.
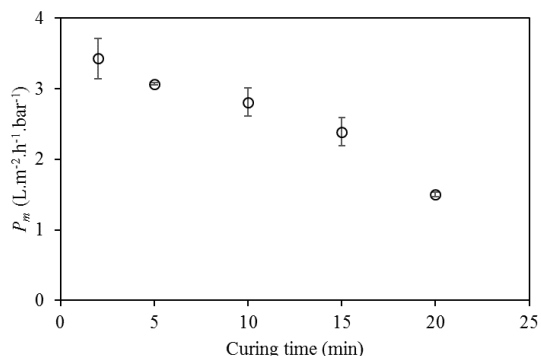
Figure 4 Effect of curing time on membrane water permeability, P_m

Figure 4 shows the P_m for membranes cured at 2, 5, 10, 15 and 20 minutes at 60 °C. P_m were reduced from 3.43 ± 0.28 L.m^{-2}.h^{-1}.bar^{-1} to 1.50 ± 0.03 L.m^{-2}.h^{-1}.bar^{-1} when the curing time were increased from 2 minutes to 20 minutes. This finding contradicted with study by Ghosh *et al.* [8] but in good agreement with other studies [9, 10]. Ghosh *et al.* [8] reported when TFC membrane were subjected to longer curing time, TFC membrane achieved higher permeability by complete evaporation of organic solvents. Here, membrane exposed to longer curing time did not have any improvement toward water permeability. A steady decrease in water permeability was observed in Figure 4 when prolonging the curing duration. The decreases in water permeability were highly

influenced by the changes to membrane's effective thickness/porosity. This trend was also observed in past study [17], where membranes with higher effective thickness/porosity have lower water permeability.

4.0 CONCLUSION

From this study, membrane cured under different curing time produces skin layer with different characteristics. It is found that a small decrease in membrane pore size when curing time was increased from 2 minute point to 10 minute point, and a small increment to pore size at 15 minute point. While, membrane effective thickness/porosity increases steadily from 2 minute point to 15 minute point. However, a huge increase in both pore size and effective thickness/porosity from 15 minute point to 20 minute point was observed. Membrane pore size and effective thickness/porosity were qualitatively related to the drying behavior of porous materials. At different level of drying, cured membranes exhibit different pore size and effective thickness/porosity that affects water permeability accordingly.

Acknowledgement

References

[1]   Siti Sabrina, M. S., Roshanida, A. S. and Norzita, N. 2013. Pretreatment of Oil Palm Fronds for Improving Hemicelluloses Content for Higher Recovery of Xylose. *Jurnal Teknologi*. 2: 39-42.

[2]   Zahari, M. A. K. M., Abdullah, S. S. S., Roslan, A. M., Ariffin, H., Shirai, Y. and Hassan, M. A. 2014. Efficient Utilization of Oil Palm Frond for Bio-based Products and Biorefinery. *Journal of Cleaner Production*. 65: 252-260.

[3]   Hassan, O., Ling, T. P., Maskat, M. Y., Illias, R. M., Badri, K., Jahim, J. and Mahadi, N. M. 2013. Optimization of Pretreatments for The Hydrolysis of Oil Palm Empty Fruit Bunch Fiber (EFBF) Using Enzyme Mixtures. *Biomass and Bioenergy*. 56: 137-146.

[4]   Feng, Y. M., Chang, X. L., Wang, W. H. and Ma, R. Y. 2009. Separation of Galacto-oligosaccharides Mixture by Nanofiltration. *Journal of the Taiwan Institute of Chemical Engineers*. 40(3): 326-332.

[5]   Sjoman, E., Manttari, M., Nystrom, M., Koivikko, H. and Heikkila, H. 2007. Separation of Xylose from Glucose By Nanofiltration From Concentrated Monosaccharide Solutions. *Journal of Membrane Science*. 292(1-2): 106-115.

[6]   Sjoman, E., Manttari, M., Nystrom, M., Koivikko, H. and Heikkila, H. 2008. Xylose Recovery by Nanofiltration from Different Hemicellulose Hydrolyzate Feeds. *Journal of Membrane Science*. 310(1-2): 268-277.

[7]   Mah, K. H., Yussof, H. W., Abu Seman, M. N. and Mohammad, A.W. 2016. Separation of Xylose Using a Thin-film Composite Nanofiltration Membrane: Screening of

[8]   Interfacial Polymerization Factors. *RSC Advances*. 6: 69454-69464.

[9]   Ghosh, A. K., Jeong, B.-H., Huang, X. and Hoek, E. M. V. 2008 Impacts of Reaction and Curing Conditions On Polyamide Composite Reverse Osmosis Membrane Properties. *Journal of Membrane Science*. 311(1-2): 34-45.

[9]   Rangarajan, R., Desai, N. V., Daga, S. L., Joshi, S. V., Prakash Rao, A., Shah, V. J., Trivedi, J. J., Devmurari, C. V., Singh, K., Bapat, P. S., Raval, H. D., Jewrajka, S. K., Saha, N. K., Bhattacharya, A., Singh, P. S., Ray, P., Trivedi, G. S., Pathak, N., Reddy, A. V. R. 2011. Thin Film Composite Reverse Osmosis Membrane Development and Scale Up at CSMCRI, Bhavnagar. *Desalination*. 282: 68-77.

[10]   Rao, A. P., Desai, N. V. and Rangarajan, R. 1997. Interfacially Synthesized Thin Film Composite RO Membranes for Seawater Desalination. *Journal of Membrane Science*. 124(2): 263-272.

[11]   Rao, A. P., Joshi, S., Trivedi, J., Devmurari, C. and Shah, V. 2003. Structure–performance Correlation of Polyamide Thin Film Composite Membranes: Effect of Coating Conditions On Film Formation. *Journal of Membrane Science*. 211(1): 13-24.

[12]   Zhao, J., Wang, Z., Wang, J. and Wang, S. 2006. Influence of Heat-treatment On CO2 Separation Performance of Novel Fixed Carrier Composite Membranes Prepared by Interfacial Polymerization. *Journal of Membrane Science*. 283(1-2): 346-356.

[13]   Mah, K. H., Yussof, H. W., Abu Seman, M. N. and Mohammad, A. W. 2016. Thin-film Composite Nanofiltration Membrane: A Study On the Curing Time and Its Performance Evaluation. *International Journal of Biomass & Renewables*. 5(1): 19-25.

[14]   Tang, B., Huo, Z. and Wu, P. 2008. Study On a Novel Polyester Composite Nanofiltration Membrane by Interfacial Polymerization of Triethanolamine (TEOA) And Trimesoyl Chloride (TMC): I. Preparation, Characterization and Nanofiltration Properties Test of Membrane. *Journal of Membrane Science*. 320(1): 198-205.

[15]   Jalanni, N. A., Abu Seman, M. N. and Faizal, C. K. M. 2013. Investigation of New Polyester Nanofiltration (NF) Membrane Fouling with Humic Acid Solution. *Jurnal Teknologi*. 65(4): 69-72.

[16]   Bowen, W., Mohammad, A. W. and Hilal, N. 1997. Characterisation of Nanofiltration Membranes for Predictive Purposes—use of Salts, Uncharged Solutes and Atomic Force Microscopy. *Journal of Membrane Science*. 126(1): 91-105.

[17]   Bowen, W. and Mohammad, A. W. 1998. Characterization and Prediction of Nanofiltration Membrane Performance-a General Assessment. *Chemical Engineering Research and Design*. 76(8): 885-893.

[18]   Bowen, W. and Sharif, A.O. 1994. Transport Through Microfiltration Membranes—Particle Hydrodynamics and Flux Reduction. *Journal of Colloid and Interface Science*. 168(2): 414-421.

[19]   Reingruber, H., Zankel, A., Mayrhofer, C. and Poelt, P. 2012. A New in Situ Method for The Characterization of Membranes in A Wet State in The Environmental Scanning Electron Microscope. *Journal of Membrane Science*. 399-400: 86-94.

[20]   Song, Y., Sun, P., Henry, L. L. and Sun, B. 2005. Mechanisms of Structure and Performance Controlled Thin Film Composite Membrane Formation Via Interfacial Polymerization Process. *Journal of Membrane Science*. 251: 67-79.

[21]   Hermans, S., Bernstein, R., Volodin, A. and Vankelecom, I. F. J. 2015. Study of Synthesis Parameters and Active Layer Morphology of Interfacially Polymerized Polyamide-polysulfone Membranes. *Reactive and Functional Polymers*. 86: 199-208.

[22]   Pinnau, I. and Freeman, B. D. 1999. Formation and Modification of Polymeric Membranes: Overview. *Membrane Formation and Modification*. 744: 1.

[23] Ismail, A. F., Padaki, M., Hilal, N., Matsuura, T. and Lau, W. J. 2015. Thin Film Composite Membrane - Recent Development and Future Potential. *Desalination*. 356: 140-148.

[24] Bruins, P. F. 1976. *Unsaturated Polyester Technology*. CRC Press.

[25] Cao, X. and Lee, L. J. 2003. Control of Shrinkage and Residual Styrene Of Unsaturated Polyester Resins Cured At Low Temperatures: I. Effect Of Curing Agents. *Polymer*. 44(6): 1893-1902.

[26] Shih, W. 1994. Shrinkage Modeling of Polyester Shrink Film. *Polymer Engineering & Science*. 34(14): 1121-1128.